

A 2D mechanical–thermal coupled model to simulate material mixing observed in friction stir welding process

S. Mesmoudi¹ · A. Timesli² · B. Braikat¹ · H. Lahmam¹ · H. Zahrouni^{3,4}

Received: 18 October 2016 / Accepted: 31 January 2017 / Published online: 23 March 2017
© Springer-Verlag London 2017

Abstract The aim of our work is the numerical modeling of two dimensional mechanical–thermal material mixing observed in stir welding process using a high order algorithm. This algorithm is based on coupling a meshless approach, a time discretization, a homotopy transformation, a development in Taylor series and a continuation method. The performance of the proposed model is the consideration of large deformations in the formulation of the posed problem. For the spatial treatment, we use the moving least squares approximation which will be applied directly to the strong form formulation of conservation equations. Each collocation point holds mechanical–thermal variables. The high order algorithm and the homotopy transformation allow reducing the number of tangent matrices to decompose and to avoid iterative procedure. Comparisons with the classical iterative solver (Jamal et al. in *J Comput Mech* 28:375–380, 2002) are performed. Numerical results reveal that a few number of matrix factorization is needed with the proposed approach, decreasing the computation time.

Keywords Friction stir welding · Material mixing · Large deformations · Mechanical–thermal behavior · Meshless method · Homotopy transformation · Taylor series

1 Introduction

Numerical simulation of friction stir welding (FSW) process is a major challenge for researchers because of the complexity of the process and the coupled physical phenomena [19]. Indeed, this process involves the coupling between mechanical, thermal and metallurgical problems. In recent literature, contributions concerning numerical modeling of FSW can be classified into two main classes. The first one uses Eulerian formulations and is based on fluid dynamics codes to study material flow around the welding tool. Usually these studies are conducted to search for stationary solution which excludes cases of welding tools with complex geometries. A second class uses the finite element method in Lagrangian formulation. It can deal with unsteady state problems considering more or less complex geometries of the tool. However, these methods suffer from the complexity of the formulation which has to manage the large deformations induced in the vicinity of the tool by re-meshing this area or using the arbitrary Lagrangian Eulerian formalism and also these methods require very large computation time making their use less convenient for the engineer. To overcome this drawback, some contributions proposed to address the problem using mesh-free methods. The aim is to avoid remeshing and then to reduce diffusion problems in the numerical solution [4, 6, 21, 22]. Some works have been done for the 3D simulation of friction stir welding using natural element method [1, 2], particle tracing method [16], finite element method [8] and particle method [9].

✉ B. Braikat
b.braikat@gmail.com

¹ Laboratoire d'Ingénierie et Matériaux LIMAT, Faculté des Sciences Ben M'Sik, Université Hassan II de Casablanca, Sidi Othman, BP 7955, Casablanca, Maroc

² Département de Génie Civil et Environnement, Ecole Nationale des Sciences appliquées (ENSA), Université Mohammed Premier, BP 03, Ajdir Al Hoceima, Maroc

³ Laboratoire d'Etude des Microstructures et de Mécanique des Matériaux LEM3, CNRS UMR 7239, Université Lorraine, Metz, Ile du Saulcy, 57045 Metz Cedex 01, France

⁴ DAMAS, Laboratory of Excellence on Design of Alloy Metals for low-mAss Structures, Université de Lorraine, Metz, France

In a previous paper [20], we have proposed a 2D mechanical formulation to model material mixing using a meshless method and a high order algorithm which is applied on a strongly formulation. Indeed, we have chosen to use the moving least squares (MLS) approximation which has been used for the first time to construct smooth functions for a scatter. This method allows to build a local approximation of the solution using low degree of polynomials whose coefficients depend on spatial coordinates. However, in the case of the element-free Galerkin method (EFG), the MLS approximation is used within a weak formulation [11, 18].

In the work [20], we have applied the algorithm on a strong form formulation of the mechanical problem to avoid difficulties related to numerical integration. As the problem is temporal, the classical implicit Euler scheme is used for the time discretization. During material mixing, the deformations are important. We therefore used a nonlinear constitutive law dependent on the strain rate. To reduce the computation time and the number of tangent matrix decompositions, we have proposed a high order algorithm. After the time discretization, the obtained nonlinear problem is transformed using the homotopy technique which consists in introducing an arbitrary matrix and a scalar parameter. If this homotopy parameter is set to zero, we obtain an easy problem to solve and when this parameter is equal to one we recover the initial problem before homotopy transformation. The solution of the modified nonlinear problem is sought by expanding the unknowns in the form of Taylor series with respect to homotopy parameter. Our experience shows that when the arbitrary matrix introduced in the modified problem is chosen judiciously, only one tangent matrix decomposition is required to compute tens of time steps which allows one to reduce significantly the total computation time.

In the present work, we propose to extend the application field of the model used in [20] to the case of 2D mechanical–thermal material mixing observed in friction stir welding process. We present the thermo-mechanical problem under a strong formulation. The coupling between the mechanical and thermal problem is due to the heat source and the law giving the viscosity depending on the temperature and the equivalent strain rate. According to these relations, the considered problem is strongly nonlinear. For the spatial discretization, we use the MLS approximation which will be applied directly to the strong form formulation. Each collocation point holds mechanical and thermal unknowns. The high order algorithm and the homotopy transformation used in [20] allow reducing the number of tangent matrices to decompose and to avoid iterative procedure. Let us recall that in the used algorithm, we did not need any iterative corrections.

The layout of this paper is as follows. In Sect. 2, we present the governing equations of the mechanical–thermal problem. We consider sticking conditions for the contact interface between welding tool and piece. In Sect. 3, we give details of the used algorithm. To search the solution in the form of power series, the different equations of the nonlinear problem are transformed in a quadratic framework. This allows the algorithm to be optimal. After that a time discretization is applied and the obtained nonlinear problem is discretized using MLS approximation. Thereafter the homotopy technique and the development in Taylor series are used in continuation procedure. In Sect. 4, numerical application is proposed and a comparison with an implicit iterative algorithm [10] based on the MLS approximation is performed to assess the validity of our algorithm. Finally, some conclusions are presented in Sect. 5.

2 Governing equations

The general laws of physics, especially the mechanics of deformable media, are based on the principle of conservation laws. This principle expresses stock of influences affecting the physical quantities such as quantity of motion, mass and energy to establish equations to solve. The resulting problem is described by the two first conservation laws for an incompressible material including:

$$\begin{cases} \rho \dot{V} = \text{div}(\sigma) \\ \text{div}(V) = 0 \end{cases} \quad (1)$$

where ρ is the material density, V is the velocity vector of components u and v , $\dot{V} = \partial V / \partial t$, σ is the stress tensor and the gravity is neglected. The constitutive law is given by the deviatoric stress tensor under the following form:

$$S = 2\mu\dot{\epsilon}, \quad (2)$$

where μ is the material dynamic viscosity and $\dot{\epsilon}$ is the strain rate tensor defined as:

$$\dot{\epsilon} = \frac{1}{2}({}^t\nabla V + \nabla V) \quad (3)$$

The equation of energy conservation, in our case, is written as follows:

$$\rho C_p \dot{T} = \text{div}(k_c \nabla T) + q_v \quad (4)$$

where T is the temperature, $\dot{T} = \partial T / \partial t$, C_p is the coefficient of specific heat, k_c is the thermal conductivity of the material and q_v denotes the volume source. This volume source q_v in the heat equation corresponding to the mechanical power dissipated per unit volume. It can be written from the velocity field of the mechanical problem as follows:

$$q_v = \beta S : \dot{\epsilon} \quad (5)$$

where β is a coefficient taken equal to 0.9. Taking into account the relation (2), the Eq. (5) can be written as follows:

$$q_v = 3\beta\mu\bar{\epsilon}^2 \tag{6}$$

where $\bar{\epsilon}$ is the equivalent strain rate given by:

$$\bar{\epsilon} = \sqrt{\frac{2}{3}\dot{\epsilon}:\dot{\epsilon}} \tag{7}$$

For the dynamic viscosity, we choose a power law as in [3] given by:

$$\mu = \frac{1}{3}KT^A\bar{\epsilon}^{n-1} \tag{8}$$

where K , A and n are the material properties. To satisfy the condition of incompressibility numerically in the Eq. (1), we introduce, in general, a pressure term penalized by a large factor noted λ . This means that the incompressibility condition (1) is replaced by a viscous law [17]:

$$p = -\lambda\text{Tr}(\dot{\epsilon}) \tag{9}$$

where $\text{Tr}(\cdot)$ denotes the trace. The stress tensor σ , under this assumption, is given by:

$$\sigma = \lambda\text{Tr}(\dot{\epsilon})I + 2\mu\dot{\epsilon} \tag{10}$$

where I is the unity tensor. Finally, the mechanical–thermal equations and the constitutive laws can be written as follows:

$$\begin{cases} \rho\dot{V} = \text{div}(\sigma) \\ \rho C_p \dot{T} = \text{div}(k_c \nabla T) + q_v \\ \sigma = \lambda\text{Tr}(\dot{\epsilon})I + 2\mu\dot{\epsilon} \\ \dot{\epsilon} = \frac{1}{2}({}^t\nabla V + \nabla V) \\ \bar{\epsilon} = \sqrt{\frac{2}{3}\dot{\epsilon}:\dot{\epsilon}} \\ \mu = \frac{1}{3}KT^A\bar{\epsilon}^{n-1} \\ q_v = 3\beta\mu\bar{\epsilon}^2 \end{cases} \tag{11}$$

The Eq. (11) will be completed by the boundary and initial conditions of mechanical and thermal type.

3 The proposed algorithm

To solve the problem (11), we propose, in this work, a high order implicit algorithm which combines: a temporal implicit scheme, a meshless approach, a homotopy transformation, a development in Taylor series and a continuation procedure. With the aim to write the problem (11) in quadratic form, we introduce the following changes of variables and the differential forms:

$$\begin{cases} \alpha = T^A \\ \gamma = \bar{\epsilon}^{n-1} \\ \varphi = \bar{\epsilon}^2 \\ Td\alpha = A\alpha dT \\ \bar{\epsilon}d\gamma = (n-1)\gamma d\bar{\epsilon} \end{cases} \tag{12}$$

Once the strongly nonlinear relationships of the problem (11) have been transformed into quadratic equations, it is easy to develop the unknown in Taylor series and to calculate numerically these series to a high order. Thus, the quadratic problem is written as:

$$\begin{cases} \rho\dot{V} = \text{div}(\sigma) \\ \rho C_p \dot{T} = \text{div}(k_c \nabla T) + q_v \\ \sigma = \lambda\text{Tr}(\dot{\epsilon})I + 2\mu\dot{\epsilon} \\ \dot{\epsilon} = \frac{1}{2}({}^t\nabla V + \nabla V) \\ \bar{\epsilon}^2 = \frac{2}{3}\dot{\epsilon}:\dot{\epsilon} \\ \mu = \frac{K}{3}\alpha\gamma \\ Td\alpha = A\alpha dT \\ \bar{\epsilon}d\gamma = (n-1)\gamma d\bar{\epsilon} \\ q_v = 3\beta\mu\varphi \\ \varphi = \bar{\epsilon}^2 \end{cases} \tag{13}$$

3.1 Temporal implicit scheme

For solving the nonlinear unsteady problem (13), we use here the Euler implicit scheme widely used in the resolution of this problems. Using the Euler implicit scheme, the time discretization of the problem (13) leads to the following nonlinear system in terms of the new unknown at time $t^{k+1} = (k+1)\Delta t$:

$$\begin{cases} \rho(V^{k+1} - V^k) = \Delta t \text{div}(\sigma^{k+1}) \\ \rho C_p (T^{k+1} - T^k) = \Delta t \text{div}(k_c \nabla T^{k+1}) + \Delta t q_v^{k+1} \\ \sigma^{k+1} = \lambda\text{Tr}(\dot{\epsilon}^{k+1})I + 2\mu^{k+1}\dot{\epsilon}^{k+1} \\ \dot{\epsilon}^{k+1} = \frac{1}{2}({}^t\nabla V^{k+1} + \nabla V^{k+1}) \\ (\bar{\epsilon}^{k+1})^2 = \frac{2}{3}\dot{\epsilon}^{k+1}:\dot{\epsilon}^{k+1} \\ \mu^{k+1} = \frac{K}{3}\alpha^{k+1}\gamma^{k+1} \\ T^{k+1}d\alpha^{k+1} = A\alpha^{k+1}dT^{k+1} \\ \bar{\epsilon}^{k+1}d\gamma^{k+1} = (n-1)\gamma^{k+1}d\bar{\epsilon}^{k+1} \\ q_v^{k+1} = 3\frac{\beta}{C_p}\mu^{k+1}\varphi^{k+1} \\ \varphi^{k+1} = (\bar{\epsilon}^{k+1})^2 \end{cases} \tag{14}$$

where $(\cdot)^{k+1}$ represent the unknowns at time $t^{k+1} = (k+1)\Delta t$ with Δt is the time step. We introduce the increments ΔV , ΔT , $\Delta\sigma$, $\Delta\dot{\epsilon}$, $\Delta\bar{\epsilon}$, $\Delta\mu$, Δq_v , $\Delta\alpha$, $\Delta\gamma$ and $\Delta\varphi$ as new unknowns of the problem (14) given by:

$$\begin{cases} \Delta V = V^{k+1} - V^k \\ \Delta T = T^{k+1} - T^k \\ \Delta \sigma = \sigma^{k+1} - \sigma^k \\ \Delta \dot{\epsilon} = \dot{\epsilon}^{k+1} - \dot{\epsilon}^k \\ \Delta \bar{\epsilon} = \bar{\epsilon}^{k+1} - \bar{\epsilon}^k \\ \Delta \mu = \mu^{k+1} - \mu^k \\ \Delta q_v = q_v^{k+1} - q_v^k \\ \Delta \alpha = \alpha^{k+1} - \alpha^k \\ \Delta \gamma = \gamma^{k+1} - \gamma^k \\ \Delta \varphi = \varphi^{k+1} - \varphi^k \end{cases} \quad (15)$$

Taking account of the Eq. (15), the problem verified by new unknowns can be written as:

$$\begin{cases} \rho \Delta V = \Delta t \operatorname{div}(\sigma^k) + \Delta t \operatorname{div}(\Delta \sigma) \\ \rho C_p \Delta T = \Delta t \operatorname{div}(k_c \nabla T^k) + \Delta t \operatorname{div}(k_c \nabla \Delta T) + \Delta t q_v^k + \Delta t \Delta q_v \\ \Delta \sigma = \lambda \operatorname{Tr}(\Delta \dot{\epsilon}) I + 2\mu^k \Delta \dot{\epsilon} + 2\dot{\epsilon}^k \Delta \mu + 2\Delta \mu \Delta \dot{\epsilon} \\ \Delta \dot{\epsilon} = \frac{1}{2} (\nabla \Delta V + \nabla \Delta V) \\ 2\bar{\epsilon}^k \Delta \bar{\epsilon} = \frac{2}{3} (2\dot{\epsilon}^k : \Delta \dot{\epsilon} + \Delta \dot{\epsilon} : \Delta \dot{\epsilon}) - \Delta \bar{\epsilon}^2 \\ \Delta \mu = \frac{K}{3} (\alpha^k \Delta \gamma + \gamma^k \Delta \alpha + \Delta \alpha \Delta \gamma) \\ T^k d\Delta \alpha = A \alpha^k d\Delta T + A \Delta \alpha d\Delta T - \Delta T d\Delta \alpha \\ \bar{\epsilon}^k d\Delta \gamma = (n-1) \gamma^k d\Delta \bar{\epsilon} + (n-1) \Delta \gamma d\Delta \bar{\epsilon} - \Delta \bar{\epsilon} d\Delta \gamma \\ \Delta q_v = 3\beta (\mu^k \Delta \varphi + \varphi^k \Delta \mu + \Delta \mu \Delta \varphi) \\ \Delta \varphi = 2\bar{\epsilon}^k \Delta \bar{\epsilon} + \Delta \bar{\epsilon}^2 \end{cases} \quad (16)$$

In the resolution, we precede to write the equations (16) a and (16)b in a single equation. Then we combine the unknowns Δu , Δv and ΔT at point x into a single vector $\{\Delta X_x\}$ given by:

$$\{\Delta X_x = {}^t \langle \Delta u, \Delta v, \Delta T \rangle\} \quad (17)$$

3.2 Moving least squares (MLS) approximation

The MLS approximation was devised by mathematicians in data fitting and surface construction [11]. It can be categorized as a method of series representation of functions. An excellent description of the MLS approximation can be

found in a paper by Lancaster and Salkauskas [11]. The MLS approximation is now widely used in MFree methods for constructing MFree shape functions. The MLS approximation of unknown vector $\{\Delta X_x\}$ is defined at point x as:

$$\{\Delta X_x\} = [\Phi(x)] \{\Delta X_m\} \quad (18)$$

where $[\Phi(x)]$ is the matrix of MLS shape functions corresponding to m nodes in the support domain of the point x and $\{\Delta X_m\}$ is the vector that collects the nodal unknowns for all the nodes in the support domain. The quantities $\{\Delta X_m\}$ and $[\Phi(x)]$ are given by:

$$\begin{cases} {}^t \{\Delta X_m\} = \langle \langle \Delta X_1 \rangle, \langle \Delta X_2 \rangle, \dots, \langle \Delta X_m \rangle \rangle \\ [\Phi(x)]_{(3 \times 3m)} = \begin{bmatrix} \Phi_1 & 0 & 0 & \dots & \Phi_m & 0 & 0 \\ 0 & \Phi_1 & 0 & \dots & 0 & \Phi_m & 0 \\ 0 & 0 & \Phi_1 & \dots & 0 & 0 & \Phi_m \end{bmatrix} \end{cases} \quad (19)$$

with Φ_i ; $i = 1 \dots m$ are the MLS shape functions. Taking account of the approximation (18) and after substitution and assembly techniques, the problem (16) is written in the following condensed form:

$$\begin{cases} [K_T^k] \{\Delta X\} + \Delta t \{F_Q(\{\Delta X\}, \{\Delta X\})\} = \Delta t \{F^k\} \\ \{\Delta \dot{\epsilon}_x\} = [B] \{\Delta X_m\} \\ 2\bar{\epsilon}_x^k \Delta \bar{\epsilon}_x = \frac{2}{3} (2^t \{\dot{\epsilon}_x^k\} [R] \{\Delta \dot{\epsilon}_x\}) + \bar{\epsilon}_x^{nl} \\ T_x^k d\Delta \alpha_x = A \alpha_x^k d\Delta T_x + \alpha_x^{nl} \\ \bar{\epsilon}_x^k d\Delta \gamma_x = (n-1) \gamma_x^k d\Delta \bar{\epsilon}_x + \gamma_x^{nl} \\ \Delta \varphi_x = 2\bar{\epsilon}_x^k \Delta \bar{\epsilon}_x + \varphi_x^{nl} \\ \Delta \mu_x = \frac{K}{3} (\alpha_x^k \Delta \gamma_x + \gamma_x^k \Delta \alpha_x) + \mu_x^{nl} \\ \{\Delta \sigma_x\} = [C^k] \{\Delta \dot{\epsilon}_x\} + \{\sigma_x^{nl}\} \\ \Delta q_v = 3\frac{\beta}{C_p} (\mu_x^k \Delta \varphi_x + \varphi_x^k \Delta \mu_x) + q_v^{nl} \end{cases} \quad (20)$$

where $[K_T^k]$ is the tangent matrix that depends on the solution at time $t^k = k\Delta t$, $\{\Delta X\}$ is the unknown global vector containing $3N_p$ components; with N_p is the total number of points, $\{F_Q(\{\Delta X\}, \{\Delta X\})\}$ is a quadratic form and $\{F^k\}$ is the right-hand side that depends on the solution at time $t^k = k\Delta t$ and $\bar{\epsilon}_x^{nl}$, α_x^{nl} , γ_x^{nl} , φ_x^{nl} , μ_x^{nl} , $\{\sigma_x^{nl}\}$ and q_v^{nl} are the quadratic terms, the vectorial quantities are given by:

$$\begin{aligned} \{\Delta \dot{\epsilon}_x\} &= \begin{Bmatrix} \Delta \dot{\epsilon}_{11} \\ \Delta \dot{\epsilon}_{22} \\ 2\Delta \dot{\epsilon}_{12} \end{Bmatrix}; \quad [B_{(3 \times 3m)}] = \begin{bmatrix} \frac{\partial \Phi_1}{\partial x} & 0 & 0 & \dots & \frac{\partial \Phi_m}{\partial x} & 0 & 0 \\ 0 & \frac{\partial \Phi_1}{\partial y} & 0 & \dots & 0 & \frac{\partial \Phi_m}{\partial y} & 0 \\ \frac{\partial \Phi_1}{\partial y} & \frac{\partial \Phi_1}{\partial x} & 0 & \dots & \frac{\partial \Phi_m}{\partial y} & \frac{\partial \Phi_m}{\partial x} & 0 \end{bmatrix} \\ \{\Delta \sigma_x\} &= \begin{Bmatrix} \Delta \sigma_{11} \\ \Delta \sigma_{22} \\ \Delta \sigma_{12} \end{Bmatrix}; \quad [C^k] = \begin{bmatrix} 2\mu^k + \lambda \left(1 - \frac{\lambda}{2\mu^k + \lambda}\right) & \lambda \left(1 - \frac{\lambda}{2\mu^k + \lambda}\right) & 0 \\ \lambda \left(1 - \frac{\lambda}{2\mu^k + \lambda}\right) & 2\mu^k + \lambda \left(1 - \frac{\lambda}{2\mu^k + \lambda}\right) & 0 \\ 0 & 0 & \mu^k \end{bmatrix} \quad (21) \\ [R] &= \begin{bmatrix} 1 & 0 & 0 \\ 0 & 1 & 0 \\ 0 & 0 & \frac{1}{2} \end{bmatrix} \end{aligned}$$

3.3 Homotopy transformation

To avoid the decomposition of the tangent matrix to each time step, we use an homotopy transformation by introducing, in the problem (20), an arbitrary matrix $[K^*]$ and an artificial parameter “ a ” under the following form:

$$\left\{ \begin{aligned} & [K^*]\{\Delta\chi(a)\} + a([K_T^k] - [K^*])\{\Delta\chi(a)\} + a\Delta t\{F_Q(\{\Delta\chi(a)\}, \{\Delta\chi(a)\})\} = a\Delta t\{F^k\} \\ & \{\Delta\dot{E}_x(a)\} = [B]\{\Delta\chi_m(a)\} \\ & 2\bar{e}_x^k \Delta\dot{E}_x(a) = \frac{4}{3} \{e_x^k\} [R]\{\Delta\dot{E}_x(a)\} + \bar{E}_x^{nl}(a) \\ & T_x^k d\Delta\Lambda_x(a) = A\alpha_x^k d\Delta T_x(a) + \Lambda_x^{nl}(a) \\ & \bar{e}_x^k d\Delta\Gamma_x(a) = (n-1)\gamma_x^k d\Delta\bar{E}_x + \Gamma_x^{nl}(a) \\ & \Delta\phi_x(a) = 2\bar{e}_x^k \Delta\bar{E}_x(a) + \phi_x^{nl}(a) \\ & \Delta MU_x(a) = \frac{K}{3} (\alpha_x^k \Delta\Gamma_x(a) + \gamma_x^k \Delta\Lambda_x(a)) + MU_x^{nl}(a) \\ & \{\Delta\Sigma_x(a)\} = [C^k]\{\Delta\dot{E}_x(a)\} + 2\Delta MU_x\{e_x^k\} + \{\Sigma_x^{nl}(a)\} \\ & \Delta Q_x^v(a) = \frac{3\beta}{C_p} (\mu_x^k \Delta\phi_x(a) + \phi_x^k \Delta MU_x(a)) + Q_x^{vnl}(a) \end{aligned} \right. \tag{22}$$

where $\{\Delta\chi(a)\}$ and the others are new unknowns of the problem (22) such that if $a = 0$ it is null and if $a = 1$ it coincides with the solution of the problem (20), the quantities $\bar{E}_x^{nl}(a)$, $\Lambda_x^{nl}(a)$, $\Gamma_x^{nl}(a)$, $\phi_x^{nl}(a)$, $MU_x^{nl}(a)$, $\{\Sigma_x^{nl}(a)\}$ and $Q_x^{vnl}(a)$ are the quadratic forms.

3.4 Development in Taylor series

The unknown of artificial problem (22) is sought here as developments in Taylor series truncated at order p with respect to homotopy parameter “ a ” in the following form:

$$\left\{ \begin{aligned} & \{\Delta\chi\} = a\{\Delta\chi_1\} + a^2\{\Delta\chi_2\} + \dots + a^p\{\Delta\chi_p\} \\ & \{\Delta\dot{E}_x\} = a\{\Delta\dot{E}_1\} + a^2\{\Delta\dot{E}_2\} + \dots + a^p\{\Delta\dot{E}_p\} \\ & \Delta\bar{E}_x = a\Delta\bar{E}_1 + a^2\Delta\bar{E}_2 + \dots + a^p\Delta\bar{E}_p \\ & \Delta\Lambda_x = a\Delta\Lambda_1 + a^2\Delta\Lambda_2 + \dots + a^p\Delta\Lambda_p \\ & \Delta\Gamma_x = a\Delta\Gamma_1 + a^2\Delta\Gamma_2 + \dots + a^p\Delta\Gamma_p \\ & \Delta\phi_x = a\Delta\phi_1 + a^2\Delta\phi_2 + \dots + a^p\Delta\phi_p \\ & \Delta MU_x = a\Delta MU_1 + a^2\Delta MU_2 + \dots + a^p\Delta MU_p \\ & \{\Delta\Sigma_x\} = a\{\Delta\Sigma_1\} + a^2\{\Delta\Sigma_2\} + \dots + a^p\{\Delta\Sigma_p\} \\ & \Delta Q_x^v = a\Delta Q_1 + a^2\Delta Q_2 + \dots + a^p\Delta Q_p \end{aligned} \right. \tag{23}$$

The developments in Taylor series (23) are introduced into the equations to be solved and by equating like powers of “ a ”, the nonlinear problem (22) is transformed into a sequence of linear ones. When the problem contains soft nonlinearity which is quadratic with respect to the

unknown $\{\chi(a)\}$, the use of developments is relatively simple and easy. The linear problems obtained at each order of truncation can be written:

$$\text{Order } 1: \left\{ \begin{aligned} & [K^*]\{\Delta\chi_1\} = \Delta t\{F^k\} \\ & \{\Delta\dot{E}_1\} = [B]\{\chi_1\} \\ & \Delta\bar{E}_1 = \frac{2}{3\bar{e}_x^k} \{e_x^k\} [R]\{\Delta\dot{E}_1\} \\ & \Delta\Lambda_1 = \frac{1}{T_x^k} A\alpha_x^k \Delta T_1 \\ & \Delta\Gamma_1 = \frac{1}{\bar{e}_x^k} (n-1)\gamma_x^k \Delta\bar{E}_1 \\ & \Delta\phi_1 = 2\bar{e}_x^k \Delta\bar{E}_1 \\ & \Delta MU_1 = \frac{K}{3} (\alpha_x^k \Delta\Gamma_1 + \gamma_x^k \Delta\Lambda_1) \\ & \{\Delta\Sigma_1\} = [C^k]\{\Delta\dot{E}_1\} + 2\Delta MU_1\{e_x^k\} \\ & \Delta Q_1 = \frac{3\beta}{C_p} (\mu_x^k \Delta\phi_1 + \phi_x^k \Delta MU_1) \end{aligned} \right. \tag{24}$$

$$\text{Order } j, 2 \leq j \leq p: \left\{ \begin{aligned} & [K^*]\{\Delta\chi_j\} = ([K^*] - [K_T^k])\{\Delta\chi_{j-1}\} + \Delta t\{F_j^{nl}\} \\ & \{\Delta\dot{E}_j\} = [B]\{\Delta\chi_j\} \\ & \Delta\bar{E}_j = \frac{2}{3\bar{e}_x^k} \{e_x^k\} [R]\{\Delta\dot{E}_j\} + \bar{E}_j^{nl} \\ & \Delta\Lambda_j = \frac{1}{T_x^k} A\alpha_x^k \Delta T_j + \Lambda_j^{nl} \\ & \Delta\Gamma_j = \frac{1}{\bar{e}_x^k} (n-1)\gamma_x^k \Delta\bar{E}_j + \Gamma_j^{nl} \\ & \Delta\phi_j = 2\bar{e}_x^k \Delta\bar{E}_j + \phi_j^{nl} \\ & \Delta MU_j = \frac{K}{3} (\alpha_x^k \Delta\Gamma_j + \gamma_x^k \Delta\Lambda_j) + MU_j^{nl} \\ & \{\Delta\Sigma_j\} = [C^k]\{\Delta\dot{E}_j\} + 2\Delta MU_j\{e_x^k\} + \{\Sigma_j^{nl}\} \\ & \Delta Q_j = \frac{3\beta}{C_p} (\mu_x^k \Delta\phi_j + \phi_x^k \Delta MU_j) + Q_j^{nl} \end{aligned} \right. \tag{25}$$

where $\{(\cdot)_j^{nl}\}$ are the second member vectors depending of terms of the lower orders of Taylor series. The previous linear problems have all the same tangent matrix which is defined by the arbitrary matrix $[K^*]$. With this technique a part of the nonlinear solution branch can be computed.

3.5 Continuation procedure

To determine the whole nonlinear solution, a continuation procedure based on the developments in Taylor series has been proposed in [5]. The key point is to define the validity range of the developments in Taylor series (23). The definition of the validity range of the Eq. (23) is easily obtained by requiring that the difference between two developments in Taylor series solutions (23) at consecutive orders remains smaller at the end of the step than a chosen parameter tolerance “ η ”. Hence, the maximum value “ a_{\max} ” of a homotopy parameter “ a ” can be defined with the following equation [5, 12–15]:

$$a_{\max} = \left(\eta \frac{\| \{ \Delta \chi_1 \} \|}{\| \{ \Delta \chi_p \} \|} \right)^{\left(\frac{1}{p-1} \right)} \tag{26}$$

For unsteady problems, the parameter “ a_{\max} ” which depends of time allows us to determine the maximum time “ t_{\max} ” of validity of the series which is defined by the following inequality:

$$a_{\max} \geq 1 \tag{27}$$

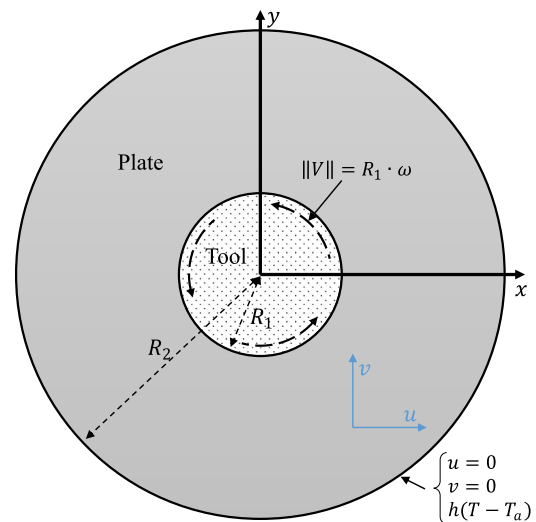
The solution of the problem (14) is obtained by writing:

$$\begin{cases} \{ X^{k+1} \} = \{ X^k \} + \{ \Delta \chi(a=1) \} \\ \{ \dot{e}_x^{k+1} \} = \{ \dot{e}_x^k \} + \{ \Delta \dot{E}_x(a=1) \} \\ \bar{e}_x^{k+1} = \bar{e}_x^k + \Delta \bar{E}_x(a=1) \\ \alpha_x^{k+1} = \alpha_x^k + \Delta A_x(a=1) \\ \gamma_x^{k+1} = \gamma_x^k + \Delta \Gamma_x(a=1) \\ \varphi_x^{k+1} = \varphi_x^k + \Delta \phi_x(a=1) \\ \mu_x^{k+1} = \mu_x^k + \Delta MU_x(a=1) \\ \{ \sigma_x^{k+1} \} = \{ \sigma_x^k \} + \{ \Delta \Sigma_x(a=1) \} \\ q_v^{k+1} = q_v^k + \Delta Q_x^v(a=1) \end{cases} \tag{28}$$

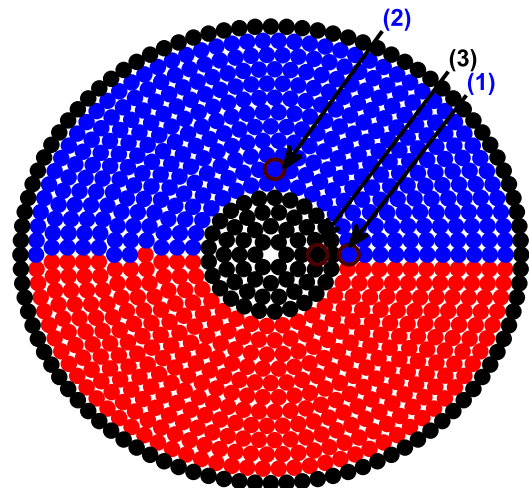
This maximum time will be considered later as an initial condition for the next step of the continuation procedure. The whole solution of the problem (20) is determined branch by branch [20].

4 Numerical application

In this section, we present a numerical analysis to demonstrate the efficiency of the algorithm derived from our numerical modeling for the simulation of friction stir welding. The area affected thermo-mechanically is assumed small compared to the area occupied by the welded plates. This area is considered as an assembly of two holed plates which have the shape of a half-disc (see Fig. 1a). These circular plates of interior radius $R_1 = 1.5$ mm and exterior radius $R_2 = 6$ mm, respectively, are made of a visco-plastic material of aluminum alloy AA7075. The interior radius



(a) The considered visco-plastic plate, its geometrical characteristics, initial and boundary conditions



(b) Initial configuration and registration points

Fig. 1 Data of considered example

R_1 corresponds here to the radius of the welding tool. The mechanical data used in this application are: for circular plates; $k = 2.69 \cdot 10^{10}$ N mm⁻², $A = -3.3155$, $n = 0.1324$, $\rho = 2780$ kg/m³, $C_p = 920$ J/kg K and $k_c = 140$ W/m K [3] and for welding tool; $\rho_t = 7800$ kg/m³,

Table 1 Influence of the truncation order p on the average validity range t_{\max} and number of steps of the proposed algorithm in the time range [0, 0.7 s].

Truncation order p	7	10	15	20
Average validity range t_{\max} (s)	0.0175	0.0185	0.0209	0.0209
Number of steps	46	43	39	39

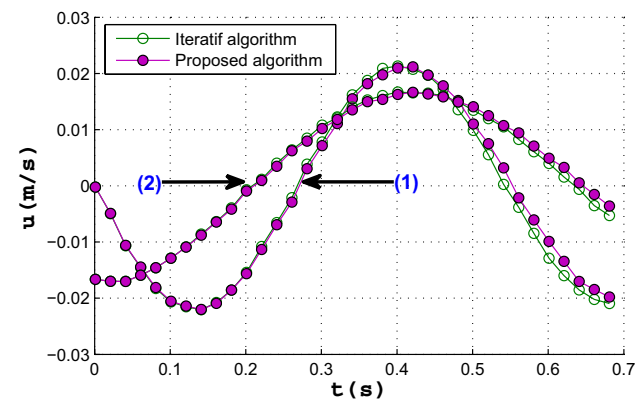
$C_{p_i} = 450 \text{ J/kg K}$ and $k_{c_i} = 36 \text{ W/m K}$. The initial and boundary conditions adopted in this example (see Fig. 1a) are given by:

$$\begin{cases} u(x, y, t) = -\sqrt{x^2 + y^2}\omega \sin(\omega t) & \text{for } x^2 + y^2 \leq R_1^2 & \text{and } \forall t \geq 0 \\ v(x, y, t) = \sqrt{x^2 + y^2}\omega \cos(\omega t) & \text{for } x^2 + y^2 \leq R_1^2 & \text{and } \forall t \geq 0 \\ u(x, y, t) = 0 & \text{for } x^2 + y^2 = R_2^2 & \text{and } \forall t \geq 0 \\ v(x, y, t) = 0 & \text{for } x^2 + y^2 = R_2^2 & \text{and } \forall t \geq 0 \\ -k_c \frac{\partial T(x,y,t)}{\partial N} = h(T(x, y, t) - T_a) & \text{for } x^2 + y^2 = R_2^2 & \text{and } \forall t \geq 0 \\ u(x, y, t) = 0 & \text{for } R_1^2 < x^2 + y^2 < R_2^2 & \text{and } t = 0 \\ v(x, y, t) = 0 & \text{for } R_1^2 < x^2 + y^2 < R_2^2 & \text{and } t = 0 \\ T(x, y, t) = 300 \text{ K} & \text{for } 0 \leq x^2 + y^2 \leq R_2^2 & \text{and } t = 0 \end{cases} \quad (29)$$

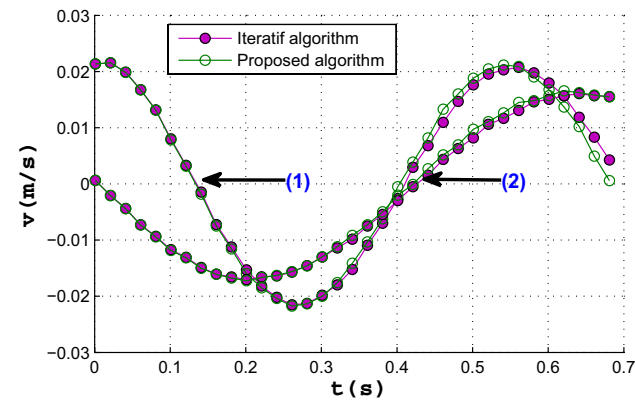
where $\omega = 20 \text{ rad/s}$ is the rotational speed of the welding tool, N is the normal to the circular contour of radius R_2 , T_a is the ambient temperature taken equal to 300 K and $h = 1000 \text{ W/m}^2 \text{ K}$ is the heat transfer coefficient.

The analysis is made in the time range $[0, 0.7 \text{ s}]$ with a time step $\Delta t = 10^{-4} \text{ s}$ for the Euler scheme. The size of

the influence domain h_1 is taken equal to $3dr$ with dr being the inter-point distance taken equal to 3.7510^{-4} m and the weight function is chosen as:



(a) Temporal evolution of the component u



(b) Temporal evolution of the component v

Fig. 2 Evolution of u and v components of the velocity vector according to the time t at the registration points (1) and (2) presented in Fig. 1b

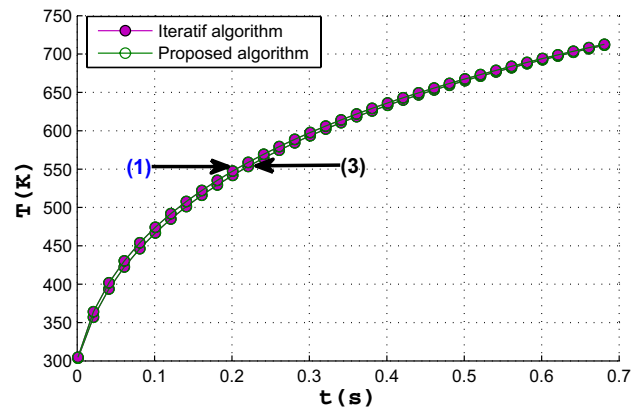


Fig. 3 Temporal evolution of the temperature T at the registration points (1) and (3) presented in Fig. 1b

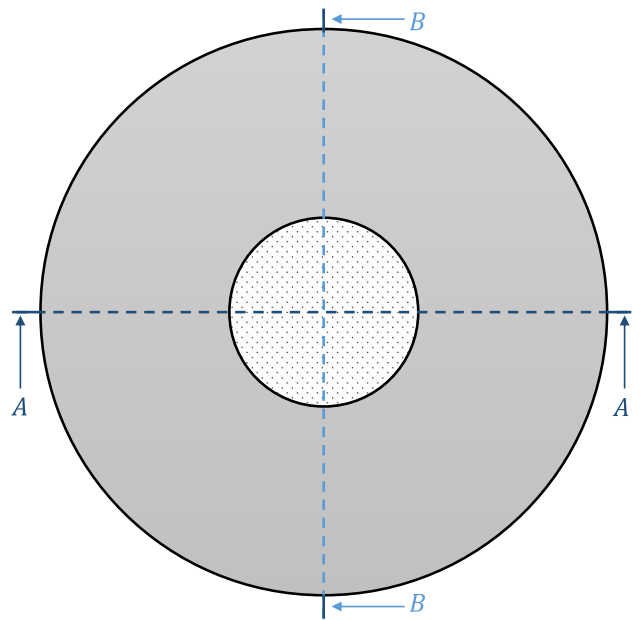
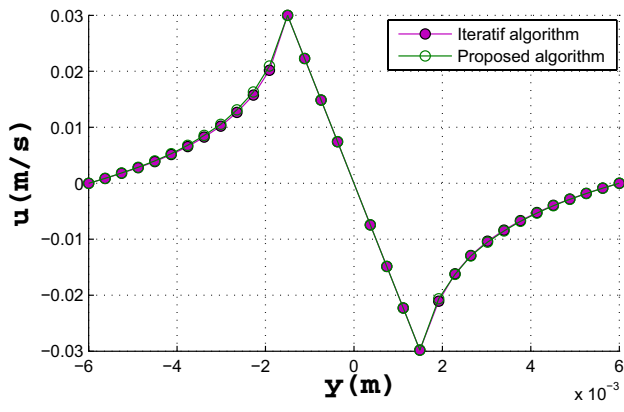
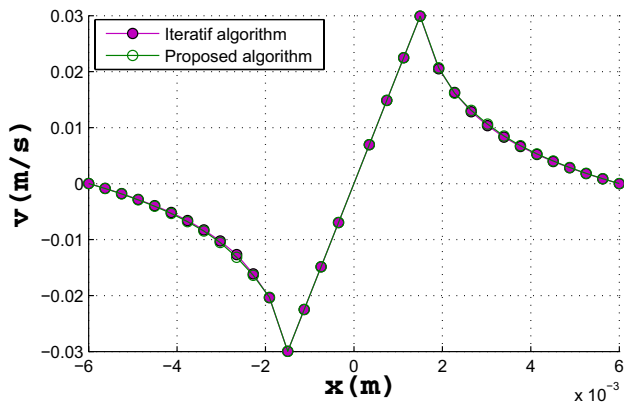


Fig. 4 Registration sections (A – A) and (B – B)



(a) Registration section (B – B)



(b) Registration section (A – A)

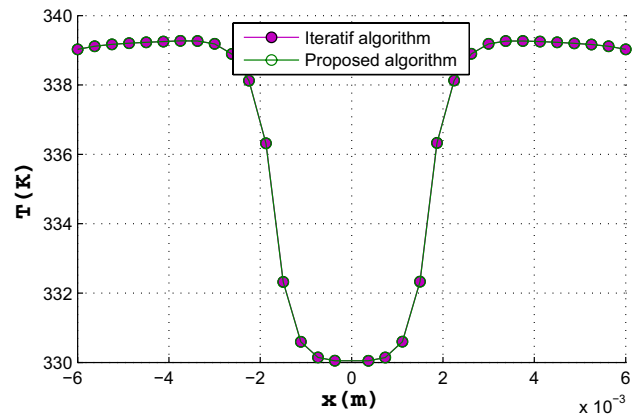
Fig. 5 Evolution of u and v components of the velocity vector according to the registration sections (B – B) and (A – A), respectively

$$w(r) = \begin{cases} e^{-(\frac{r}{c})^{2q}} & \text{if } r \leq 1 \\ 0 & \text{if } r > 1 \end{cases} \quad (30)$$

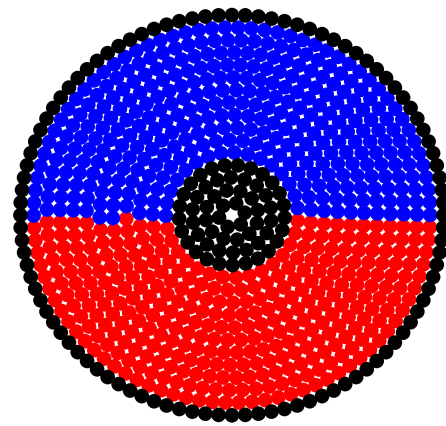
where $r = \|x - x_m\| / h_l$, $c = 0.2$ and $q = 1$. With these data, the area occupied by the plates which are represented by colors blue and red, respectively and the welding tool is replaced by 846 points (see Fig. 1b). The pre-conditioner matrix $[K^*]$ is taken equal to the tangent matrix $[K_T^{t_{max}}]$ evaluated at the started time of each step.

In this application, we will discuss the influence of the truncation order p on the maximum time t_{max} during a step of the continuation technique. The Table 1 shows that when the truncation order p increases the size of the average validity range t_{max} increases and stabilizes from the truncation order $p = 15$ for a fixed tolerance parameter $\eta = 10^{-6}$. Similarly, if we increase the order of truncation the number of steps of the proposed algorithm decreases and stabilizes from the order $p = 15$ (see Table 1).

After these numerical tests we choose thereafter the truncation order $p = 7$ and the tolerance parameter $\eta = 10^{-6}$ for the proposed algorithm and the tolerance



(a) Registration section (A – A) or (B – B)

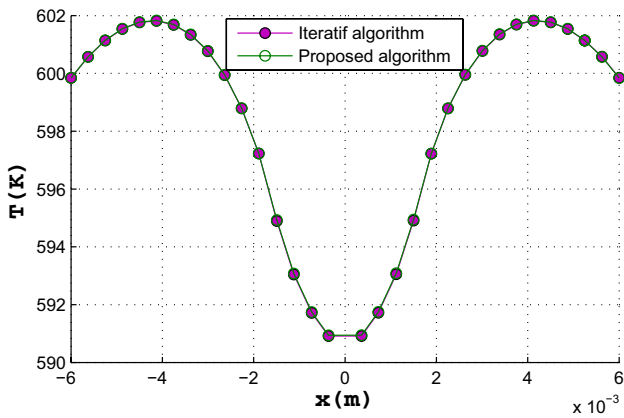


(b) Material mixing state

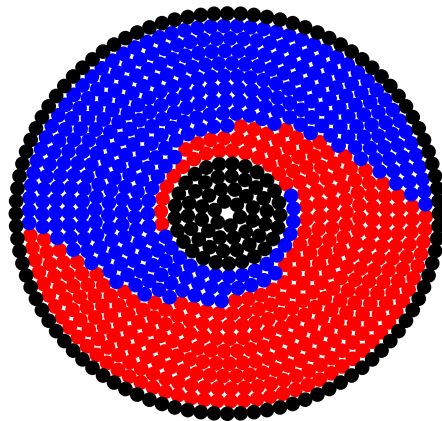
Fig. 6 Evolution of the temperature T along the registration section (A – A) and material mixing state at time $t = 0.01$ s.

parameter $\delta = 10^{-6}$ for the iterative method. The obtained solution is compared with that obtained by the conventional method using the Euler scheme coupled with an iterative method [21] similar to that used in various areas of physics [7], it is described in [10]. In this iterative method, the convergence is evaluated by assuming that the relative difference between two consecutive iterations is less than a given tolerance parameter. The two plates are stained with the colors blue and red, respectively, to show the material mixing.

In Fig. 2, we plot the evolution of u and v components of the velocity along the time axis t at points (1) and (2) near the tool (see Fig. 1b), obtained by the proposed algorithm and the iterative method. We remark that the two solutions are confounded. It is worth noting that the solution obtained by the proposed algorithm requires 46 steps of continuation (46 inversions of the matrix $[K^*]$), whereas that obtained by the iterative method requires 15,000 inversions of matrix $[K^*]$.



(a) Registration section (A – A) or (B – B)



(b) Material mixing state

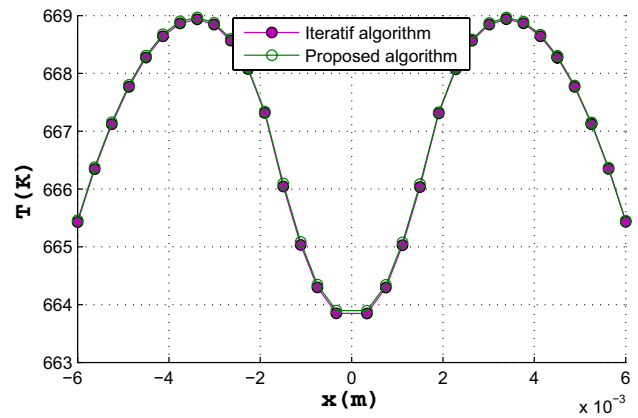
Fig. 7 Evolution of the temperature T along the registration section (A – A) and material mixing state at time $t = 0.3$ s.

Also, the Fig. 3 represents the evolution of the temperature T along the time axis t at points (1) and (3) (see Fig. 1b). The solutions obtained by the two algorithms are in good agreement. From this figure, we see that the temperature saved at point (1) is greater than that saved at point (3). This is due to the deformations which are stronger near the welding tool.

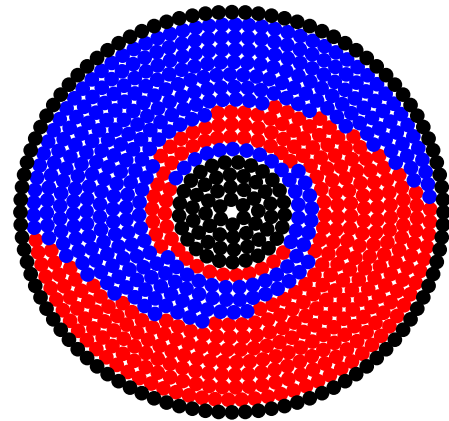
Thereafter, we proceed to make the registration sections of the components of the velocity and temperature on the lines $y = 0, x \in [-R_2, R_2]$ (A – A) and $x = 0, y \in [-R_2, R_2]$ (B – B) (see Fig. 4).

The Fig. 5 shows the evolution of u and v along the horizontal and vertical sections and the comparison between the proposed algorithm and the iterative algorithm at time $t = 0.7$ s. One can observe that the two algorithms are in good agreement.

The Figs. 6, 7, 8 and 9 show the evolution of temperature T along the horizontal section or vertical section and the state of material mixing at times $t = 0.01$ s, $t = 0.3$ s, $t = 0.5$ s and $t = 0.7$ s, respectively. From these figures,



(a) Registration section (A – A) or (B – B)



(b) Material mixing state

Fig. 8 Evolution of the temperature T along the registration section (A – A) and material mixing state at time $t = 0.5$ s.

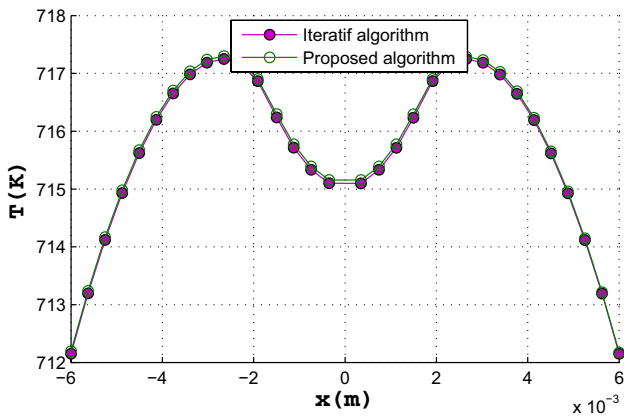
we remark that the material flow (deformation) is circular about the tool because the mixing process is controlled only by rotating speed.

The Fig. 10 shows the temperature distribution T at time $t = 0.001$ s and $t = 0.7$ s, respectively.

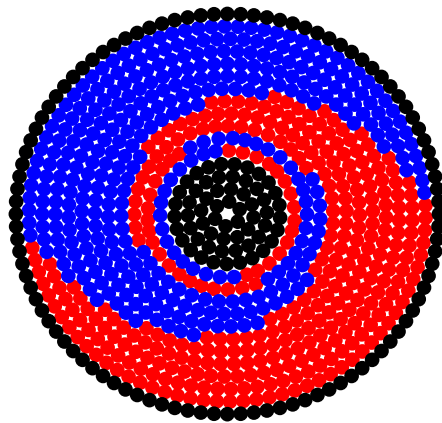
The Fig. 11 illustrates the temperature distribution in the welded plate and in the considered tool for times $t = 0.05$ s and $t = 0.08$ s. The temperature distribution is symmetric because the heat generation near the tool during the mixing process is dominated by rotating speed of the tool.

5 Conclusion

In this work, we have used the high order algorithm for the simulation of mechanical–thermal material mixing observed during the FSW process in the bi-dimensional



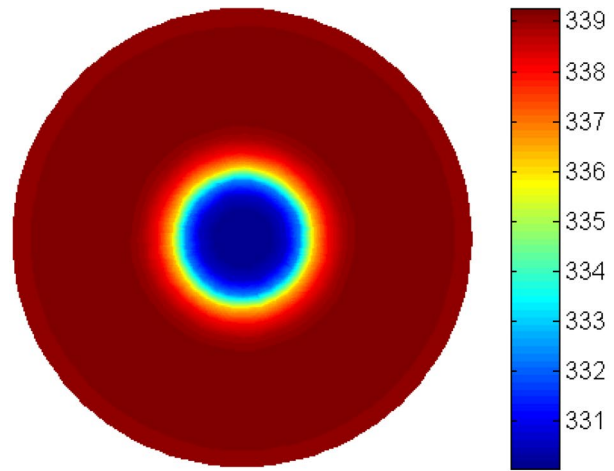
(a) Registration section ($A - A$) or ($B - B$)



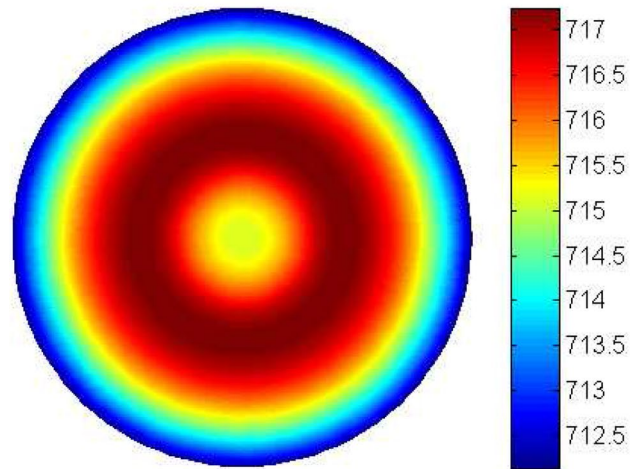
(b) Material mixing state

Fig. 9 Evolution of the temperature T along the registration section ($A - A$) and material mixing state at time $t = 0.7$ s.

case. This algorithm combines the high order implicit technique based on developments in Taylor series and meshless method based on MLS. A mechanical–thermal formulation is used under a strong form. The obtained results are convincing compared to the iterative method. The used algorithm requires no correction and one inversion of the iteration matrix allows us to get a good part of the solution. The key points in this high order implicit algorithm are, first a high order solver based on developments in Taylor series, second the possibility of choosing the tangent matrix $[K^*]$ which limits the number of matrices to be triangulated. Let us recall that the used algorithm solves the nonlinear visco-plastic problem with a high order predictor without any correction. The used algorithm can easily be adapted to other nonlinear problems. This comparison confirms the robustness, accuracy and efficiency of the algorithm. Compared to the iterative method, the algorithm is found competitive in terms of computational cost versus accuracy, and benefit from a simple implementation. This work is currently in



(a) At time $t = 0.001$ s



(b) At time $t = 0.7$ s

Fig. 10 Temperature distribution at times $t = 0.001$ s and $t = 0.7$ s

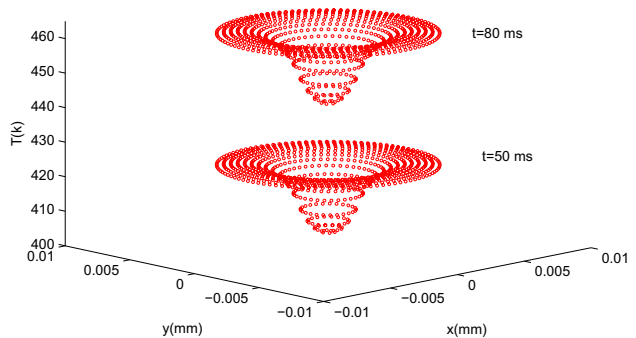


Fig. 11 Temperature distribution at times $t = 0.05$ s and $t = 0.08$ s

progress to other application fields as the three-dimensional mixing process.

Compliance with ethical standards

Conflict of interest The authors, Said Mesmoudi, Abdelaziz Timesli, Bouazza Braikat, Hassane Lahmam and Hamid Zahrouni, declare that there is no conflict of interest concerning the publication of the article entitled “A 2D mechanical–thermal coupled model to simulate material mixing observed in friction stir welding process” and this article is original and never published. We look forward to hearing from you.

References

- Alfaro I, Fratini L, Cueto E, Chinesta F (2008) Numerical simulation of friction stir welding by natural element methods. *Int J Mater Form* 1(1):1079–1082
- Alfaro I, Racineux G, Poitou A, Cueto E, Chinesta F (2009) Numerical simulation of friction stir welding by natural element methods. *Int J Mater Form* 2(2):225–234
- Buffa G, Hu J, Shivpuri R, Fratini L (2006) A continuum based on fem model for friction stir welding model development. *Mater Sci Eng* 419:389–396
- Canales D, Cueto E, Feulvarch E, Chinesta F (2014) First steps towards parametric modeling of fsw processes by using advanced separated representations: numerical techniques. *Key Eng Mater* 611–612:513–520
- Cochelin B (1994) A path following technique via an asymptotic numerical method. *J Comput Struct* 53:1181–1192
- Cueto E, Chinesta F (2015) Meshless methods for the simulation of material forming. *Int J Mater Form* 8(1):25–43
- Fornberg B, Whitham GB (1978) A numerical and theoretical study of certain nonlinear wave phenomena. *Philos Trans R Soc Lond A: Math Phys Sci* 289:373–404
- He X, Gu F, Ball A (2014) A review of numerical analysis of friction stir welding. *Prog Mater Sci* 65:1–66
- Hirasawa S, Badarinarayan H, Okamoto K, Tomimura T, Kawanami T (2010) Analysis of effect of tool geometry on plastic flow during friction stir spot welding using particle method. *J Mater Process Technol* 210(11):1455–1463
- Jamal M, Braikat B, Boutmir S, Damil N, Potier-Ferry M (2002) A high order implicit algorithm for solving instationary non-linear problems. *J Comput Mech* 28:375–380
- Lancaster P, Salkauskas K (1981) Surfaces generated by moving least squares methods. *Math Comput* 37(155):141–158
- Mhada K, Braikat B, Hu H, Damil N, Potier-Ferry M (2012) About macroscopic models of instability pattern formation. *Int J Solids Struct* 49(21):2978–2989
- Mottaqui H, Braikat B, Damil N (2010) Discussion about parameterization in the asymptotic numerical method: application to nonlinear elastic shells. *Comput Methods Appl Mech Eng* 199:1701–1709
- Mottaqui H, Braikat B, Damil N (2010) Local parameterization and the asymptotic numerical method. *Math Model Nat Phenom* 5:16–22
- Potier-Ferry M, Damil N, Braikat B, Descamps J, Cadou JM, Cao HL, Elhage Hussein A (1997) Traitement des fortes non linéarités par la méthode asymptotique numérique. *Comptes Rendus de l’Académie des Sciences Paris* 324(3):171–177
- Haider A, Taqi AC, Ho-Sung Y, Younghae D, Cheol WP (2015) Numerical prediction of algae cell mixing feature in raceway ponds using particle tracing methods. *Biotechnol Bioeng* 112(2):297–307
- Odin G, Savoldelli C, Boucharda PO, Tillier Y (2010) Determination of Young’s modulus of mandibular bone using inverse analysis. *Med Eng Phys* 32(6):630–637
- Shivanian E (2016) More accurate results for two-dimensional heat equation with Neumann’s and non-classical boundary conditions. *Eng Comput* 32(4):729–743
- Thomas WM, Nicholas ED, Needham JC, Church MG, Temple-Smith P, Dawes C (1991) Friction stir butt welding. International Patent Application no. PCT/GB92/02203 and GB Patent Application no. 9125978.8
- Timesli A, Braikat B, Lahmam H, Zahrouni H (2015) A new algorithm based on moving least square method to simulate material mixing in friction stir welding. *J Eng Anal Bound Elem* 50:372–380
- Timesli A, Braikat B, Zahrouni H, Moufki A, Lahmam H (2013) An implicit algorithm based on continuous moving least square to simulate material mixing in friction stir welding process. *J Model Simul Eng* 2013:14
- Yoshikawa G, Miyasaka F, Hirata Y, Katayama Y, Fuse T (2012) Development of numerical simulation model for fsw employing particle method. *Sci Technol Weld Join* 17(4):255–263